available at www.sciencedirect.com

ScienceDirect

journal homepage: www.elsevier.com/locate/ecolmodel

A size-resolved pelagic ecosystem model

Mark E. Baird[a,*], *Iain M. Suthers*[b]

[a] *Climate and Environmental Dynamics Laboratory, School of Mathematics and Statistics, University of NSW, Sydney, NSW 2052, Australia*

[b] *School of Biological, Earth and Environmental Sciences, University of NSW, Sydney, NSW 2052, Australia*

ARTICLE INFO

Article history:
Received 30 November 2005
Received in revised form
10 November 2006
Accepted 13 November 2006
Published on line 8 January 2007

Keywords:
Plankton
Size
Biomass size spectrum
Zooplankton
Protozoa
Metazoa

ABSTRACT

A size-resolved pelagic ecosystem model is developed using descriptions of physical limits to biological processes and allometric relationships to determine physiological rates. The model contains three functional groups: phytoplankton, protozoans and metazoans—requiring three separately resolved size distributions. Within each functional group the size-resolution of the model can be altered without changing the model parameters, which are the coefficients of the allometric relationships, or changing the model equations, which are characteristic of each functional group. This approach allows the number of size-classes to be varied, and for a convergence of output with increasing resolution to be achieved.

In this paper, a biological configuration is analysed composed of 62 size-classes doubling in biomass between classes and ranging in volume over 19 orders of magnitude from 0.32 μm^3, representative of the cyanobacteria *Prochlorococcus* sp., to 2.05×10^{18} μm^3, representative of a metazoan size-class with an equivalent spherical radius of 78.8 cm. The phytoplankton size-classes extend through the first 17 size-classes, protozoan from the 9th to 21st, and metazoan from the 18th to 62nd. The size-resolved model is coupled to a 1D model of the oceanic mixed layer. Numerical experiments show the size-resolved model is relatively insensitive to size resolution and higher order closure terms with the 62 size-class configuration, but is sensitive to initial conditions. The model output is most sensitive to the parameter describing the smallest size-class of prey available to a metazoan predator, and the nitrogen content of a phytoplankton cell. The concentration of DIN and biomass of protozoa are in general the most sensitive model outputs. These experiments provide a background understanding for further application of the size-resolved pelagic ecosystem model.

1. Introduction

Pelagic ecosystems consist of planktonic organisms of a range of sizes, the distribution of which has general trends throughout the world's oceans (Sheldon et al., 1972). These trends led oceanographers to routinely take size-based measurements of biota and to analyse the distribution of biomass with size. This methodology of analysis, called the biomass spectrum, has now been applied for over 25 years (Platt and Denman, 1977; Silvert and Platt, 1978; Heath, 1995; Zhou and Huntley, 1997; Kerr and Dickie, 2001).

The dependence of physiological rates on body size has been observed throughout the animal kingdom (Fenchel, 1974; Peters, 1983) and is known to be important in planktonic communities (Platt and Denman, 1977). The size-based dependence of planktonic interactions is also well documented,

* *Corresponding author.*
E-mail address: m.baird@unsw.edu.au (M.E. Baird).
0304-3800/$ – see front matter © 2006 Elsevier B.V. All rights reserved.
doi:10.1016/j.ecolmodel.2006.11.025

and includes studies on nutrient uptake (Hein et al., 1995), light capture (Morel et al., 1993), growth (Gillooly, 2000), grazing selection (Caparroy et al., 2000), grazing rates (Hansen et al., 1997), sinking (Kiørboe, 1993), swimming (Sommer, 1988), and copepod fecundity (Kiørboe and Sabatini, 1995). The size-structure of planktonic communities arises from an interaction of size-dependent physiological rates and planktonic interactions (Hansen et al., 1994; Kerr and Dickie, 2001).

The dynamic modelling of pelagic ecosystems has traditionally been based on food webs with fixed trophic positions (Steele and Henderson, 1981; Fasham, 1993; Taylor and Stephens, 1993), a history of which is detailed in Gentleman (2002). Recently, trophic modelling has been extended to include multiple size classes, with ecological parameters estimated from size-based studies (Moloney and Field, 1991; Gin et al., 1998; Armstrong, 1999, 2003). These size-structured models are an important step to including the effects of plankton size in pelagic ecosystem models. However, size-structured trophic models do not intrinsically incorporate a major paradigm of biological oceanography: namely that as a first approximation, the rate of physiological processes and planktonic interactions of a particular organism depends more on its size than on the trophic position of the adult stage. Using such an approximation, a 3 mm fish larvae will have a diet, predators, swimming speeds and physiological rates more in common with a 3 mm adult copepod than with its own 30 cm adult form. Furthermore, the choice of a finite set of classes in a size-structured model determines the model equations and parameter values that are used. The ability of a size-structured model to investigate the effects of size therefore depends on changing the set of model equations.

This paper formulates an ecosystem model, which focuses on plankton size as the primary underlying influence on ecosystem structure. The formulation of the model, and the determination of the parameter values, is independent of the actual size-classes which are used to implement the numerical solution of the model. The number of size-classes is determined by the model resolution rather than the model structure, and as such the pelagic ecosystem model will be referred to as a size-resolving pelagic ecosystem model, borrowing from the terminology of spatially resolved in the hydrodynamic modelling literature.

In order to achieve a size-resolved model, three fundamental changes will be made when compared to existing size-structured trophic models. Firstly, following Baird and Emsley (1999) and Baird et al. (2004), physical descriptions of planktonic interactions will be used to explicitly represent the size-dependencies of limiting physical processes to ecological interactions. Physical descriptions include, for example, calculating the encounter rates of predators and prey based on the physical properties of the fluid and the geometric properties of the organism (Jackson, 1995). Secondly, physiological rates are calculated from allometric relationships found in the literature. In one sense, the parameter values of the model become the coefficients in the allometric relationships themselves, and are therefore independent of the size-resolution used in the model. Thirdly, a distinction is made in the model between animals that reproduce through division, the protozoa, and those that grow between different life stages, the metazoa. The consideration of the flux of biomass through metazoan size-classes due to the growth of individuals is a fundamental aspect of the biomass size spectra from which this paper borrows a number of ideas.

In this paper, a size-resolved pelagic ecosystem model framework is developed using physical descriptions of limits to biological processes and allometric relationships to determine physiological rates. A biological grid is outlined that contains 62 size-classes. The grid extends from $0.32\,\mu m^3$, representative of the cyanobacteria *Prochlorococcus* sp., to $2.05 \times 10^{18}\,\mu m^3$, representative of a metazoan size-class with an equivalent spherical radius of 78.8 cm. The size-resolved model is coupled to a 1D physical model of the ocean mixed layer. Numerical experiments are used to investigated the sensitivity of the model output in the surface mixed layer to (1) initial conditions, (2) size resolution, (3) the metazoan largest size-class boundary (or the higher order closure terms), and (4) the allometric relationships that determine physiological rates and planktonic interactions.

2. The physical model

The physical model is a 1D configuration of the Princeton Ocean Model (POM) which has a free surface and solves the non-linear primitive equations on sigma coordinates using finite difference methods (Blumberg and Mellor, 1987). As such, the model allows only vertical mixing forced by a sinusoidally oscillating wind with a strength varying between −0.05 and 0.05 Pa over a 3-day period. The vertical profile for vertical diffusivity, turbulent dissipation rate, solar radiation and wind-driven velocity over a 4-day period (200 days after the simulation begins) are given in Fig. 1. The light values can be seen to repeat each day, while the mixing and turbulence parameters undergo a 3-day oscillation in accordance with the 3-day period of the wind stress. The wind-driven velocity induces a velocity shear that affects the calculation of the turbulence state variables such as vertical diffusivity and turbulent dissipation rate, but there is no advection in the model.

The physical model is a 1D version of the configuration described in greater detail in Baird et al. (2004).

3. The size-resolved pelagic ecosystem model

The size-resolved model is first presented as a set of equations describing the phytoplankton, protozoan and metazoan groups. The phytoplankton growth equations look similar to the NPZ model of Baird et al. (2004), as the differential equations at any size depend only on the properties of the phytoplankton at that size, and the nutrient concentration. In contrast, the protozoan and metazoan predation terms and the metazoan growth terms depend on a range of sizes. To be formulated in the continuous form, they look quite different to the size-structured trophic models, and have more similarities with the biomass size spectrum literature (Silvert and Platt, 1978; Zhou and Huntley, 1997).

The model is integrated by resolving the phytoplankton, P, into $\mathcal{P}$ size-classes, $P_1, P_2, \ldots, P_{\mathcal{P}}$, the protozoan into $\mathcal{Z}$ size-classes, $Z_1, Z_2, \ldots, Z_{\mathcal{Z}}$, and the metazoan, G, into $\mathcal{G}$ size-classes,

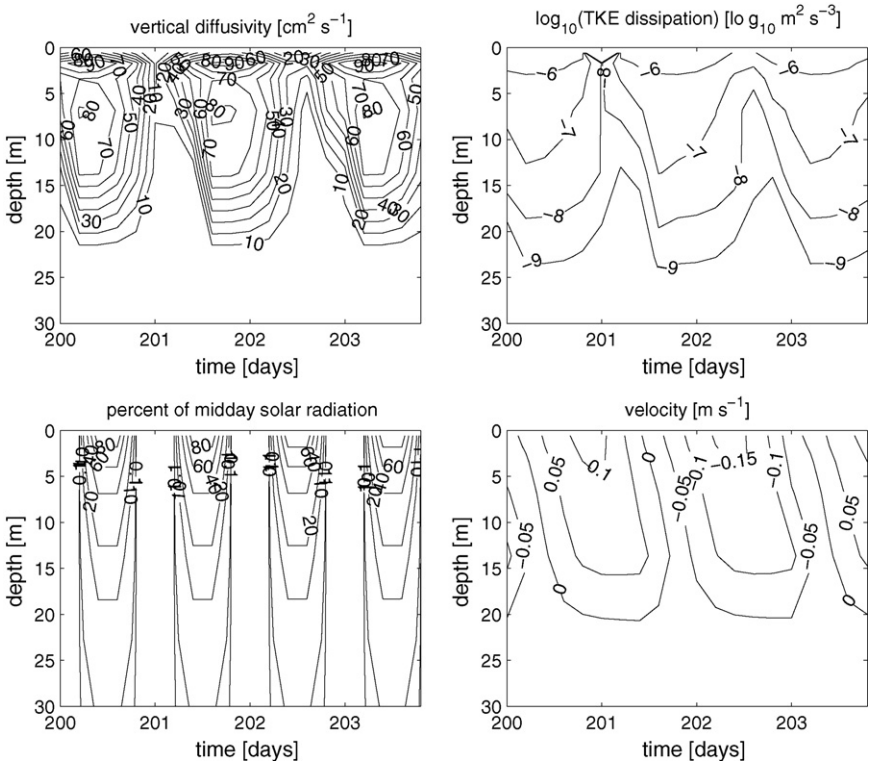

Fig. 1 – The vertical diffusivity, dissipation rate of turbulent kinetic energy, solar radiation as a percentage of the midday sun at the surface, and the wind driven horizontal velocity that force the biological model.

$G_1, G_2, \ldots, G_{\mathcal{G}}$. The state variables P_n, Z_n and G_n have units of mol N m^{-3}. The phytoplankton have an associated state variable for the nitrogen reserves, $R_{N,1}, R_{N,2}, \ldots, R_{N,\mathcal{P}}$ and energy reserves, $R_{I,1}, R_{I,2}, \ldots, R_{I,\mathcal{P}}$, which have units of mol N cell^{-1} and mol photon cell^{-1}, respectively. Fig. 2 illustrates the interactions between phytoplankton, protozoa and metazoa, with the individual terms for 8th phytoplankton class, 4th protozoan class and the 5th metazoan class in the 62 size-class configuration.

The protozoa and metazoa are defined by a variety of characteristics (Marshall and Williams, 1972). Naturally, the model must represent functional groups in restrictive ways that represent only an abstraction of the complexity associated with the natural assemblages of organisms. In the model, the protozoa reproduce by division and do not vary in size throughout their life-cycle. In contrast, the metazoa develop from an embryotic stage through approximately two orders of magnitude of length to the adult size, and involves, for the organisms considered here, the broadcasting of eggs. In terms of the model, growth of protozoa does not involve movement of mass to larger size-classes, while metazoan growth does. The following section describes the size-resolved terms for phytoplankton, protozoan and metazoan organisms.

3.1. *Phytoplankton growth*

The local rates of change of dissolved inorganic nitrogen (DIN), N, phytoplankton biomass, P, and the reserves of nitrogen, R_N, and energy, R_I for the growth of phytoplankton within the mass range $m - \Delta m$ and $m + \Delta m$ [mol N cell^{-1}], where Δm is small, are given by:

$$\frac{\partial N}{\partial t} = \underbrace{-\int_{m-\Delta m}^{m+\Delta m} k_N(m') \left(\frac{R_N^{\max}(m') - R_N(m')}{R_N^{\max}(m')} \right) \frac{P(m')}{m_{P,N}} \, dm'}_{\text{uptake by phytoplankton between } m-\Delta m \text{ and } m+\Delta m} \tag{1}$$

$$\frac{dR_N(m)}{dt} = \underbrace{+k_N(m) \left(\frac{R_N^{\max}(m) - R_N(m)}{R_N^{\max}(m)} \right)}_{\text{DIN uptake of size-class } m} \underbrace{- \mu_P^{\max}(m)(m_{P,N} + R_N(m)) \frac{R_N(m)}{R_N^{\max}(m)} \frac{R_I(m)}{R_I^{\max}(m)}}_{\text{loss to phytoplankton growth of size-class } m} \tag{2}$$

$$\frac{dR_I(m)}{dt} = \underbrace{+k_I(m) \left(\frac{R_I^{\max}(m) - R_I(m)}{R_I^{\max}(m)} \right)}_{\text{light capture of size-class } m} \underbrace{- \mu_P^{\max}(m)(m_{P,I} + R_I(m)) \frac{R_N(m)}{R_N^{\max}(m)} \frac{R_I(m)}{R_I^{\max}(m)}}_{\text{loss to phytoplankton growth of size-class } m} \tag{3}$$

$$\frac{\partial}{\partial t} \int_{m-\Delta m}^{m+\Delta m} P(m') \, dm' = \underbrace{+ \int_{m-\Delta m}^{m+\Delta m} \mu_P^{\max}(m') \frac{R_N(m')}{R_N^{\max}(m')} \frac{R_I(m')}{R_I^{\max}(m')} P(m') \, dm'}_{\text{growth by phytoplankton between } m-\Delta m \text{ and } m+\Delta m} \tag{4}$$

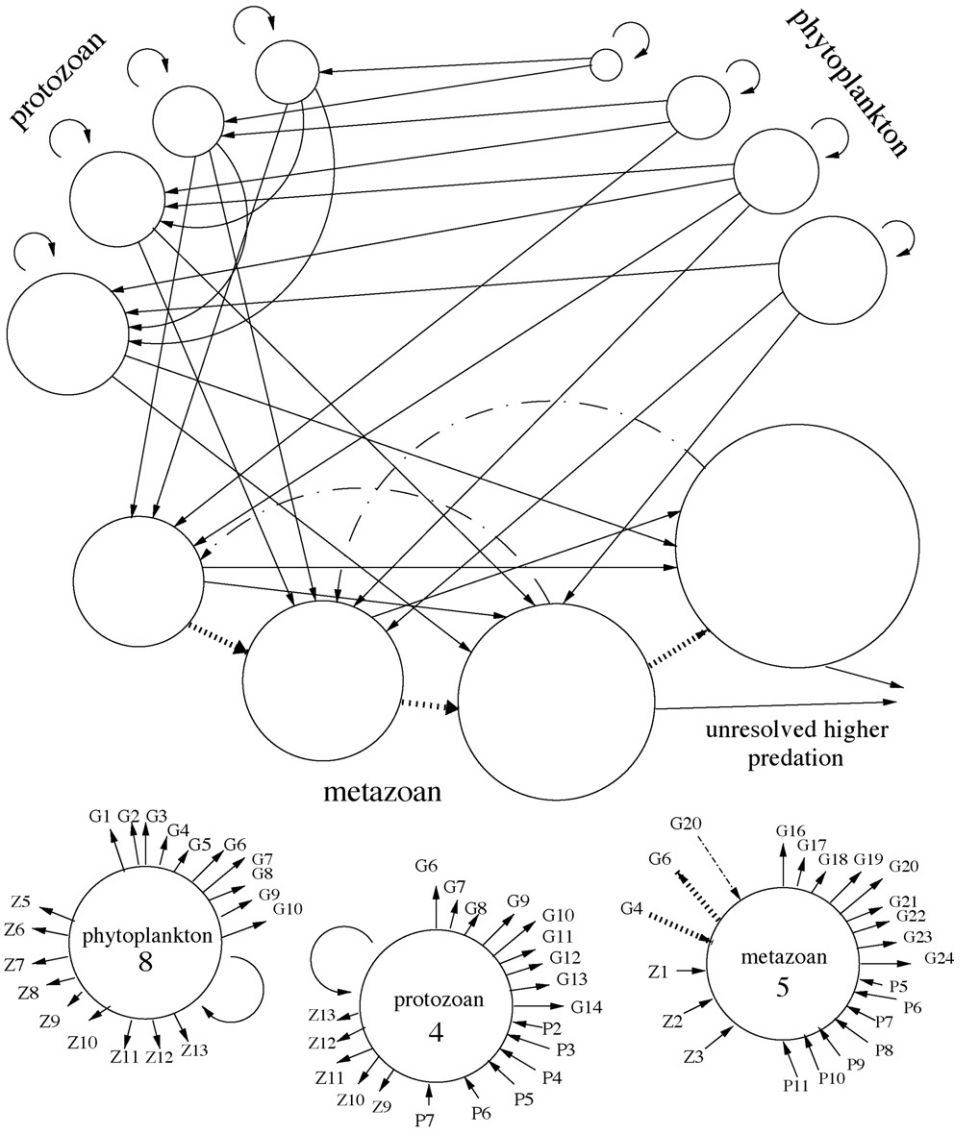

Fig. 2 – Schematic of the size-resolved biological model. The phytoplankton and protozoan groups divide, as represented by the arrow turned on itself. Growth of individuals between metazoan size-classes is represented by dashed arrows, while spawning of eggs by metazoa is represented by dot-dashed lines. All other lines are predation terms. In the top schematic, predation is limited to just two size-classes of predators within each functional group, although the 62 size-class configuration typically has 9–11. In the lower schematic, all interactions are given for the 8th phytoplankton class, 4th protozoan class and the 5th metazoan class in the 62 size-class configuration. The largest 15 metazoans have unresolved loss terms, which are modelled implicitly using a quadratic loss term that returns nitrogen to the dissolved inorganic nitrogen pool.

where k_N and k_I are the maximum rates of DIN and energy uptake of phytoplankton, respectively (and are a function of N and incident light, respectively), R_N^{max} and R_I^{max} the maximum values of R_N and R_I, respectively, and μ_P^{max} is the maximum growth rate of phytoplankton. The local time derivatives of N and P have units of mol N m^{-3} s^{-1}, while R_N has units of mol N $cell^{-1}$ s^{-1}, and R_I has units of mol photon $cell^{-1}$ s^{-1}.

For comparison, a commonly used alternate term for quantifying nitrogen reserves is total algal nitrogen or the cell quota, Q_N [mol N $cell^{-1}$], which is given by $Q_N = m_{P,N} + R_N$, where $m_{P,N}$ is the stoichiometry coefficient of nitrogen in phytoplankton, and represents the minimum quantity of nitrogen for which a cell remains viable. The parameter $m_{P,N}$ is obtained from Table 1 using the Redfield ratio (C:N = 106:16, Redfield et al., 1963). The analogous coefficient for light energy, $m_{P,I}$, is based on the quantum yield of photosynthesis. The theoretical maximum quantum yield is 0.125 mol C (mol photon)$^{-1}$, although a more realistic value of 0.1 mol C (mol photon)$^{-1}$ has been used (Kirk, 1994). The term $P/m_{P,N}$ which appears in the DIN uptake and the phytoplankton grazing terms, is the number of phytoplankton cells. A more detailed analysis, including a derivation of conservation of mass of Eqs. (1)–(4) are given in Baird et al. (2004).

Table 1 – Allometric relationships for phytoplankton

Parameter	Allometric relationship	Units	n
Carbon content[a]	$m_{P,C} = 2.12(\times/\div 2.46)V_P^{0.761\,(\pm 0.0272)}$	mol C cell^{-1}	37
Chlorophyll concentration[b]	$C = 2.06 \times 10^7(\times/\div 1.36)(10^{18}V_P)^{-0.320\,(\mp 0.035)}$	mg Chl a m^{-3}	16
Maximum growth rate[c]	$\mu_P^{max} = 3.46(\times/\div 1.16)(10^{18}V_P)^{-0.15\,(\mp 0.019)}$	day^{-1}	126
Sinking velocity[d]	$w_P = 5.60(\times/\div 2.29)r_P^{1.17\,(\pm 0.071)}$	m s^{-1}	22
Swimming velocity[e]	$U_P = 0.00272(\times/\div 6.43)r_P^{0.229\,(\pm 0.155)}$	m s^{-1}	19

Allometric coefficients are reported with standard errors. The far right column gives the sample size, n, from which the allometric relationship are determined. The nitrogen content of a phytoplankton cell is calculated using the Redfield ratio: $m_{P,N} = (16/106)m_{P,C}$. Note that for the maximum growth rate, μ_P^{max}, and the cellular chlorophyll concentration, C, the slope is $\mp$ standard error as $\log_{10}(10^{18}V_P) > 1$.

[a] Mullin et al. (1966).
[b] Finkel (2001).
[c] Tang (1995).
[d] Live cells in Smayda (1970).
[e] Marine flagellates in Sommer (1988).

Turbulence enhanced nutrient uptake by phytoplankton. In the Baird et al. (2004) NPZ model, the phytoplankton considered were small, and the effects of turbulence on nutrient uptake were not included. In the Baird et al. (2004) NPZ model, the uptake rate coefficient, k_N, was simply given by $4\pi rDN$ where r is the radius of the phytoplankton, D the molecular diffusivity of the nitrate ion and N is the dissolved inorganic nitrogen concentration. For the larger phytoplankton considered here, turbulence may enhance uptake. The uptake rate coefficient for a phytoplankton cell including the effect of turbulence is based on the work of Batchelor (1980), and is given by:

$$k_N = 4\pi rD\left(1 + 0.55\left(\frac{r^2}{D}\sqrt{\frac{\epsilon}{\upsilon}}\right)^{1/3}\right)N \tag{5}$$

where ϵ is the rate of dissipation of turbulent kinetic energy and υ is the dynamic viscosity of the water. As an example, a cell of $r = 30\,\mu$m in water of $\epsilon = 2 \times 10^{-5}\,\mathrm{m^2\,s^{-3}}$ and $\upsilon = 10^{-6}\,\mathrm{m^2\,s^{-1}}$ with a molecular diffusivity of $19 \times 10^{-10}\,\mathrm{m^2\,s^{-1}}$, the enhancement of nutrient uptake due to turbulence is 70%.

Size-dependent light capture. The uptake rate coefficient for light capture, k_I, is given by:

$$k_I = \overline{aA}I, \quad \overline{aA} = \pi r^2\left(1 - \frac{2(1-(1+2\gamma Cr)\,\mathrm{e}^{-2\gamma Cr})}{(2\gamma Cr)^2}\right) \tag{6}$$

where $\overline{aA}$ is the absorption cross-section of a phytoplankton cell [m^2 cell^{-1}], r the equivalent spherical radius, C the size-dependent intracellular chlorophyll concentration (Table 1), and $\gamma = 0.04\,\mathrm{m^2\,(mg\,Chl\,}a\mathrm{)^{-1}}$ is the chlorophyll-specific absorption coefficient (Finkel and Irwin, 2000).

The light attenuation coefficient through a layer of water, K_d, is given by:

$$K_d = k_w + \sum_{P=1}^{\mathcal{P}} n_P\overline{aA}_P \tag{7}$$

where $k_w = 0.04\ \mathrm{m^{-1}}$ is the attenuation coefficient of the water excluding phytoplankton, n_P the concentration of phytoplankton cells, and is given by $n_P = P/m_{P,N}$. The calculation of K_d using the absorption cross-section for each size class of phytoplankton accounts for the packaging of pigment within discrete cells (Kirk, 1994). The light at the bottom of a layer dz thick is given by:

$$I_{bot} = I_{top}\,\mathrm{e}^{-K_d\,dz} \tag{8}$$

and the average light within the layer is given by:

$$I = \frac{I_{top} - I_{bot}}{K_d\,dz} \tag{9}$$

3.2. Predation

Metazoan and protozoan organisms obtain their biomass from consuming other metazoan, protozoan as well as phytoplankton individuals. First the prey ranges need to be considered.

3.2.1. Prey selectivity by size

In the size-resolved model, predators select prey based on size, which affects the rate at which they encounter prey, the range of prey they choose, and the rate at which they can ingest the prey. Grazing rates are based on the minimum of the rate at which predators encounter prey within the size range available to the predator, and the prey-saturated maximum growth rate of the predator.

The encounter rate calculations are based on the curvilinear formulations of Jackson (1995) and include the effect of the size of the predator and prey on encounters. This is quantified as the encounter rate coefficient, ϕ(pred, prey), which is given by the sum of encounters due to diffusion, relative velocity (due to swimming and sinking) and turbulent shear:

$$\phi = \phi_{diffusion} + \phi_{rel.\ vel.} + \phi_{shear} \tag{10}$$

where r_{pred} and r_{prey} are the radii of the predator and prey, $p = r_{prey}/r_{pred}$, $r_{pred} > r_{prey}$, $\phi_{diffusion} = (2k_BT/3\eta)(1/r_{prey} + 1/r_{pred})(r_{prey} + r_{pred})$, $\phi_{rel.\ vel.} = 0.5\pi r_{prey}^2 U$, and $\phi_{shear} = 9.8(p^2)/((1+2p)^2)(\epsilon/\nu)^{0.5}(r_{prey} + r_{pred})^3$. The symbol ν is the kinematic viscosity, η the dynamic viscosity, $k_B = 1.38 \times 10^{-23}\,\mathrm{J\,K^{-1}}$ the Boltzmann constant, U the relative encounter velocity and ϵ is the rate of dissipation of turbulent kinetic energy (for more information see Baird et al., 2004).

For metazoa grazing on other metazoans, the ability to search for prey enhances encounters beyond the calculated random encounters above. Using physiological arguments, Ware (1978) calculated that the cross-sectional area of the

Table 2 – Allometric relationships for protozoa

Parameter	Allometric relationship	Units	n
Carbon content[a]	$m_{Z,C} = 1.29\,(\pm 0.168) \times 10^5 V_Z$	$\mathrm{g\,C\,cell^{-1}}$	9
Swimming speed[b]	$U_Z = 0.0885(\times/\div 9.91) r_Z^{0.553\,(\pm 0.195)}$	$\mathrm{m\,s^{-1}}$	21
Sinking speed[c]	$w_Z = 5.60(\times/\div 2.29) r_Z^{1.17\,(\pm 0.071)}$	$\mathrm{m\,s^{-1}}$	22
Maximum growth rate[d]	$\mu_Z^{\max} = 0.00271(\times/\div 3.31) r_Z^{-0.529\,(\pm 0.101)}$	$\mathrm{day^{-1}}$	41
Yield[e]	$\gamma_Z = 0.308\,(\pm 0.0266)$	$\mathrm{mol\,mol^{-1}}$	14
Minimum predator–prey size ratio[f]	$\Re_{Z,\min} = 3.00\,(\pm 0.930)$	–	4
Maximum predator–prey size ratio[g]	$\Re_{Z,\max} = 22.6\,(\pm 8.01)$	–	3

Allometric coefficients are reported with standard errors. The far right column gives the sample size, n, from which the allometric relationship is determined. The nitrogen content of the protozoans is calculated using the Redfield ratio: $m_{Z,N} = (16/106) m_{Z,C}$.

[a] Flagellate and ciliate categories in Hansen et al. (1997).
[b] Flagellate and ciliate categories in Hansen et al. (1997).
[c] Sinking velocity uses the same relationship as for phytoplankton.
[d] Flagellate and ciliate categories in Hansen et al. (1997).
[e] Flagellate and ciliate categories in Hansen et al. (1997).
[f] Hansen et al. (1994).
[g] Hansen et al. (1994).

reactive field of a visual predator, γ, to be:

$$\gamma = m^{0.69} \tag{11}$$

The encounter rate with searching is then given by γU, where U is the swimming speed of the predator.

Beyond the encounter rate calculations, further size selection by predators can occur as a result of, for example, geometric constraints of the feeding apparatus (Hansen et al., 1994). Size selection beyond encounter rate effects are quantified by the effectiveness of encounters, Φ(pred, prey), which takes a value between 0 and 1. When Φ(pred, prey) is equal to 0, the prey is outside the size range of the predator's diet. The effective encounter rate between predators and prey becomes Φ(pred, prey)ϕ(pred, prey).

In this paper, Φ has been set to 1 if the prey is within a set size range of the predator, and zero outside this range:

$$\Phi = 1 \quad \text{if } \Re_{\min} < \frac{r_{\text{pred}}}{r_{\text{prey}}} < \Re_{\max} \quad \text{else } \Phi = 0 \tag{12}$$

where $\Re_{\min}$ and $\Re_{\max}$ are the minimum and maximum ratios of predator to prey radius. The parameters $\Re_{\min}$ and $\Re_{\max}$ are characteristic of the predator, and are given for protozoans and metazoans in Tables 2 and 3.

3.2.2. *Prey selectivity in saturated predator growth*

The total effective encounters experienced by a predator normalised to its biomass m is given by:

Table 3 – Allometric relationships for metazoa

Parameter	Allometric relationship	Units	n
Carbon content[a]	$m_{G,C} = 1.24\,(\pm 0.109) \times 10^5 V_G$	$\mathrm{g\,C\,cell^{-1}}$	9
Swimming speed[b]	$U_G = 4.74(\times/\div 1.10) r_G^{0.838\,(\pm 0.0171)}$	$\mathrm{m\,s^{-1}}$	143
Egg size[c]	$m_{C,\bigcirc} = 0.0138(\times/\div 1.26) m_{C,\female}^{0.621\,(\pm 0.057)}$	$\mu\mathrm{g\,C}$	41
Egg production rate[d]	$\Lambda = 0.336(\times/\div 1.20) m_{C,\female}^{-0.262\,(\mp 0.067)}$	$\bigcirc\,\female^{-1}\,\mathrm{day^{-1}}$	35
Maximum growth rate[e]	$\mu_g^{\max} = 1.02(\times/\div 1.40)(1000 V_G)^{-0.37\,(\pm 0.032)}$	$\mathrm{year^{-1}}$	31
Yield[f]	$\gamma_G = 0.341\,(\pm 0.0179)$	$\mathrm{mol\,mol^{-1}}$	12
Fraction of adult females[g]	$\lambda_{Gn} = 1/12$	–	1
Minimum predator–prey size ratio[h]	$\Re_{G,\min} = 10.26\,(\pm 1.31)$	–	15
Maximum predator–prey size ratio[i]	$\Re_{G,\max} = 90.73\,(\pm 14.20)$	–	20

Allometric coefficients are reported with standard errors. The far right column gives the sample size, n, from which the allometric relationship is determined. The nitrogen content of the metazoans is calculated using the Redfield ratio: $m_{G,N} = (16/106) m_{G,C}$. Metazoans are assumed to have a zero sinking velocity, $w_G = 0$. Symbols in the units represent numbers of eggs, $\bigcirc$, and numbers of females, $\female$.

[a] Hansen et al. (1997).
[b] Swimming speed for rotifer, meroplankton larvae and copepod categories are obtained from Hansen et al. (1997), and the cruising speed of other metazoans from Huntley and Zhou (2004) (see Fig. 3).
[c] Egg size and egg production of metazoans based on broadcast spawners (Kiørboe and Sabatini, 1995).
[d] Egg size and egg production of metazoans based on broadcast spawners (Kiørboe and Sabatini, 1995).
[e] Banse and Mosher (1980).
[f] Hansen et al. (1994).
[g] Fraction of sexually mature adult females, λ_{Gn} is based on the calanoid copepod *Centropages typicus* (Bonnet and Carlotti, 2001).
[h] Hansen et al. (1994).
[i] Hansen et al. (1994).

$$T(m) = \underbrace{\int_1^{\mathcal{P}} \frac{\Phi(m,x)\phi(m,x)P_x}{m_{P,N}(x)}\,dx}_{\text{prey on phytoplankton}} + \underbrace{\int_1^{\mathcal{Z}} \frac{\Phi(m,x)\phi(m,x)Z_x}{m_{Z,N}(x)}\,dx}_{\text{prey on protozoa}} + \underbrace{\int_1^{\mathcal{G}} \frac{\Phi(m,x)\phi(m,x)G_x}{m_{G,N}(x)}\,dx}_{\text{prey on metazoa}} \quad (13)$$

The rate of effective encounters between predators and prey can be greater than that required to maintain the maximum growth rate of the predator. When the sum of effective encounters from all prey types exceeds the maximum growth rate by a factor of $1/\chi$, the grazing rate on each prey is given by χ of the maximum effective encounter rate. The fraction of the total effective encounters with that are ingested a predator is given by:

$$\chi(m) = \max\left[1, \frac{T(m)}{\mu^{\max}(m)/(1-\gamma(m))}\right] \quad (14)$$

The term $(1-\gamma(m))$ is the assimilation efficiency of the predator and accounts for increased encounters required to obtain maximum growth rate for predators that are inefficient at assimilating prey.

3.3. Protozoan growth

Protozoan growth, like phytoplankton growth, is an exponential function of biomass. The growth of protozoans within the mass range $m-\Delta m$ and $m+\Delta m$ [mol N cell^{-1}] is given by:

$$\frac{\partial}{\partial t}\int_{m-\Delta m}^{m+\Delta m} Z(m')\,dm' = \int_{m-\Delta m}^{m+\Delta m} (1-\gamma(m'))\chi(m')T(m')Z(m')\,dm' \quad (15)$$

3.4. Metazoan growth and reproduction

Metazoan life-cycles involve growing over many orders of magnitude from an egg to an adult capable of reproduction. Biomass moves up the metazoan size-classes through growth of individuals and predation on smaller prey. Biomass moves down the metazoan size-classes by the spawning of eggs, and is returned to the dissolved inorganic nitrogen pool through mortality.

The rate of change of metazoan biomass as a result of growth of individuals is given by:

$$\frac{\partial G(m)}{\partial t} = -\frac{\partial m(\chi(m)T(m) - \lambda(m)\min(\Lambda(m), \chi(m)T(m)))G(m)}{\partial m} \quad (16)$$

where λ is the fraction of sexually mature females among individuals of biomass m and Λ is the fecundity of adult females. For the calanoid copepod *Centropages typicus* with a sex ratio of 1:1, and a life cycle in which they are sexually mature for approximately 1/6th of their life (Bonnet and Carlotti, 2001), λ would take a maximum value, $\lambda^{\max}$, of 1/12. Normally a significant fraction of the eggs spawned do not make it to sexual maturity, so λ can be significantly less than a $\lambda^{\max}$.

For the sexually mature females, all of ingested biomass is allocated to producing eggs, up to a maximum determined from an allometric relationship for egg production, Λ, and the size of the adult. A further allometric relationship is used to determine the radius of the metazoan size-class, r_{egg}, to which the biomass spawned is allocated (Table 3). Any growth of sexually mature females above the maximum egg production rate is allocated to growth.

3.5. Metazoan upper boundary condition

Typically, trophically structured and size-structured models include a higher order mortality term, to which the solution is often quite sensitive (Edwards and Yool, 2000). The equivalent to the higher-order closure term in the size-resolved approach can be considered as the upper boundary of the metazoans. Since the phytoplankton and protozoan top size-classes have all their largest predators resolved, only the metazoan boundary is open. That is, the metazoan upper boundary has a flux through it to unresolved (because they are larger than the largest size class) predators, or to the dissolved inorganic nitrogen pool. The metazoan upper boundary condition is represented as a quadratic mortality term for size-classes close to the boundary which do not have all their predators resolved:

$$\frac{\partial}{\partial t}\int_{m-\Delta m}^{m+\Delta m} G(m')\,dm' = -\int_{m-\Delta m}^{m+\Delta m} \xi_{G(m')}G(m')^2\,dm' \quad (17)$$

where ξ_G is the quadratic mortality coefficient. The quadratic mortality rate, $\xi_G G^2$, is set to be equal to the maximum growth rate at the initial biomass of the metazoan size-class multiplied by the fraction of predators unresolved, ϑ:

$$\xi_{G(m)}G(m)^2 = \vartheta(m)\mu^{\max}_{G(m)}G(m), \quad \text{so } \xi_{G(m)} = \frac{\vartheta\mu^{\max}_{G(m)}}{G(m)} \quad (18)$$

Given sufficient prey, the quadratic mortality terms will relax the biomass of the largest metazoan size-classes to that of the initial conditions. In the 62 size-class configuration described below, the largest seven metazoan have all of their predators unresolved, while the 15th (ESR = 2.5 cm) to 8th (ESR = 12.4 cm) largest have some fraction of their predators unresolved. The largest 7 and 15 metazoan size-classes make up only 11.29% and 24.19%, respectively, of the total initial biomass in the system.

3.6. Biological parameter values

The relationships used to calculate model parameters for phytoplankton, protozoa and metazoa are given in Tables 1–3, respectively. All parameters values have been sourced from laboratory measurements published in the literature.

Most parameter values are determined over a range of sizes with the parameter value often varying with size. All size dependencies have been fitted to a power law relationship of the form:

$$\log_x y = (a \pm a_{S.E.}) + (b \pm b_{S.E.})\log_x r \quad (19)$$

where y is the dependent variable, a and b are coefficients with standard errors of $a_{S.E.}$ and $b_{S.E.}$, respectively, r is a measure of size, such as radius or volume, and x is the base of the logarithm. Raising both sides to the power x, the equation becomes:

$$y = x^{(a\pm a_{S.E.})}r^{(b\pm b_{S.E.})} = (x^a \times / \div x^{a_{S.E.}})r^{(b\pm b_{S.E.})} \quad (20)$$

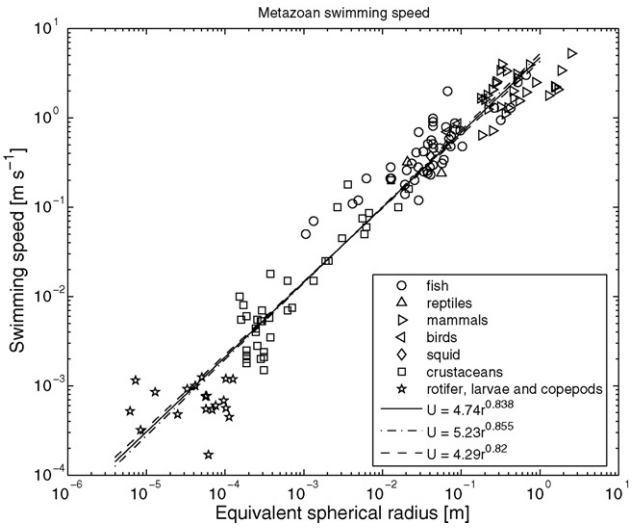

Fig. 3 – Allometric relationship for metazoan swimming speed. Rotifer, meroplankton larvae and copepod categories from Hansen et al. (1997) and cruising speed of Huntley and Zhou (2004) for all other animals. The best fit (solid line), and the best fit plus the standard error (dash-dot) and minus the standard error (dashed) are shown.

The symbol $\times/\div$ has been introduced as an analog of the symbol $\pm$. Note that Tables 1–3 report the allometric relationships as power laws. For $\log_x r < 1$, an increase in the slope will correspond in an increase in the intercept if the two fits are to both pass through the mean value of $\log r$. Alternatively for $\log_x r > 1$ the intercept will go in the opposite direction to the change in slope, as can be seen for the maximum growth rate of phytoplankton, and the chlorophyll content of a phytoplankton cell in Table 1. The sensitivity of the allometric relationships is assessed by varying both the slope and intercept together, rather than separately. So the power law above (Eq. (20)) is assessed at the limits of $(x^a \times x^{a_{S.E.}})r^{(b+b_{S.E.})}$ and $(x^a \div x^{a_{S.E.}})r^{(b-b_{S.E.})}$, where $\log_x r < 1$, or $(x^a \times x^{a_{S.E.}})r^{(b-b_{S.E.})}$ and $(x^a \div x^{a_{S.E.}})r^{(b+b_{S.E.})}$, where $\log_x r > 1$. An example of the allometric relationships is given in Fig. 3.

The dark lines in Fig. 4 illustrate the allometric relationships that are used for the standard run, while the light lines show the relationships with the slope and intercept co-varied by the standard error. The figure shows the allometric relationships over the full range of size-classes used in the model. To interpret Fig. 4, look for the spread of the standard error lines, and the size-class at which the lines intersect (noting that size-independent relationships such as metazoan yield do not intersect). The spread of lines shows the uncertainty in the parameter value, with, for example, the phytoplankton swimming speed (Fig. 4E) being less certain than the phytoplankton sinking rate (Fig. 4D). The size at which the lines intersect indicates the mid-point of the allometric relationship. For an

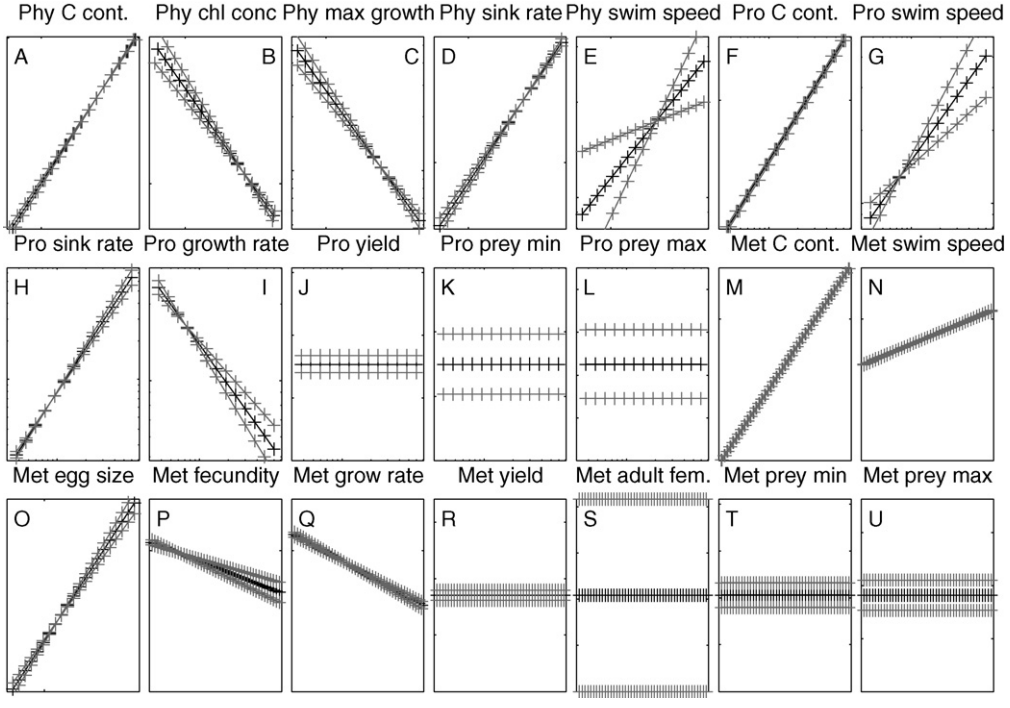

Fig. 4 – Schematic of the 21 allometric relationships used in the model (Phy, phytoplankton; Pro, protozoa; Met, metazoa). The black central line is the standard value and the grey lines represent the values used in the sensitivity analysis with the slope and intercept co-varied. All horizontal axes are logarithmically scaled size-class. Note that the yield and maximum predator–prey ratios for both protozoa and metazoa (Panels J, K, L and R, T, U, respectively), and the fraction of metazoan adult females (S) are independent of size. For these variables, the vertical axes scale between zero and twice the mean value and the vertical axes are linear. For the relationships dependent on size the vertical axis is logarithmic. The equations for these lines can be found in Tables 1–3. For more information see Section 3.6.

intersection close to the centre of the x-axis the range of the allometric relationship closely matches the size-classes in the model. For example, protozoan growth rate (Fig. 4I) is poorly centred, with the allometric relationship being based on organisms that are on average smaller than the model size-classes, while phytoplankton swimming speed (Fig. 4E) is quite well centred. The equations for these lines can be found in Tables 1–3.

3.7. The 62 size-class biological configuration

The numerical experiments conducted in this paper are based on a biological configuration with a total of 62 size-classes, with biomass doubling between size-classes. The smallest size-class is an organism with a biomass of 1.39×10^{-15} mol N, and represents a phytoplankton cell with an equivalent spherical radius by volume (ESR) of 0.32 μm such as the cyanobacteria *Prochlorococcus* sp. The largest size-class has a biomass of 3.19×10^{3} mol N and represents a metazoan size-class with an ESR of 78.8 cm. The model contains 17 phytoplankton, 13 protozoan and 45 metazoan size-classes, a total of 75 classes of organisms represented. The largest nine phytoplankton classes overlap with the smallest nine protozoan classes, and the largest four protozoan classes overlap with the smallest four metazoan classes, resulting in a total of 62 size-classes.

The phytoplankton are represented in the first 17 size-classes, with biomass ranging from 1.39×10^{-15} to 9.07×10^{-11} mol N cell^{-1} and representing cells of ESR from 0.32 μm to 41.0 μm. The largest size is representative of a diatom such as *Stephanodiscus* (Graham and Wilcox, 2000).

The protozoans are represented in the 9th to 21st size-class. The 9th size-class has a biomass of 3.54×10^{-13} mol N cell^{-1} and is representative of a 3.74 μm ESR protozoan cell such as the nanoflagellate *Paraphysomonas* sp. (Hansen et al., 1997). The largest class of protozoa has an ESR of 60.0 μm, representative of a dinoflagellate such as *Protoperidinium* sp. or the ciliate *Flavella ehrenbergii* (Hansen et al., 1997).

The metazoans are represented in the 18th to 62nd size-classes. The 18th size-class has an ESR of 30.3 μm and is representative of the eggs of a small metazoa such as *Paracalanus parvus* (Kiørboe and Sabatini, 1995). The first 13 metazoan size-class are composed only of eggs, larvae and juveniles and do not spawn eggs. The 30th metazoan is representative of a metazoan with an ESR of 2.46 cm such as an adult anchovy (www.fishbase.net). The 62nd size-class has a volume of 2 m^3, and represents large animals such as marine mammals. The biological grid is extended up to the 62nd size class in order to resolve all the predators of the first 25th metazoan classes. The 25th metazoan class ($r = 7$ mm) is chosen as it representative of approximately the maximum size class (larval fish) that the model is assessed, and is used in the sensitivity analysis of the top metazoan boundary condition.

3.8. The normalised biomass size spectra

To summarise the large quantity of model output, properties of the normalised biomass size spectra (NBSS) are analysed. The NBSS is a natural framework to use because the ecosystem model has been developed using a similar underlying approach and the NBSS has been used for many years to summarise the size distribution of field data.

Following Platt and Denman (1977), the normalised biomass, $\beta(w)$ is the total biomass $b(w)$ in the size-class characterised by weight w, divided by the width of the size-class Δw:

$$\beta(w) = \frac{b(w)}{\Delta w} \tag{21}$$

A commonly analysed feature of size distribution is the mean slope of the normalised biomass spectrum, given by:

$$S = \overline{\left(\frac{\partial \ln \beta}{\partial \ln w}\right)} \tag{22}$$

Observations suggest a value of S between −1.5 and −0.6 for marine waters depending on environmental conditions (Zhou, 2006), with a median around −1.0 (Sheldon et al., 1972; Kerr and Dickie, 2001).

3.9. Biological initial conditions

The biological initial conditions are determined by setting the total biomass of phytoplankton, protozoa and metazoa, TN_i, and the slope of the NBSS, S_i. In the overlap between phytoplankton and protozoans, and protozoans and metazoans, the biomass is shared equally between the overlapping functional groups. The total biomass is set to a depth-resolved annual average of the waters off the coast of NSW, Australia, following Baird et al. (2004), and the initial slope of the biomass spectra, $S_i = -1.0$, a value typical of oligotrophic waters.

A slope of the biomass spectra of −1.0 implies equal biomass in all size-classes. Including the effect of the overlap of ranges of phytoplankton, protozoa and metazoa, the initial conditions start with 20.16% of the biomass in the phytoplankton group, 10.48% in the protozoan group, and 69.35% in the metazoan group.

4. Results

The model output is averaged over an inertial period ($= |2\pi/f| = 1.028$ day^{-1}, where $f = -7.07 \times 10^{-5}$ s^{-1} is the Coriolis parameter at 30° S), to highlight the development of subinertial phenomena (Edwards et al., 2000). Fig. 5 plots the time evolution of the surface total nitrogen, DIN concentration, and the concentration of each phytoplankton, protozoan and metazoan size-class, as well as the slope of the NBSS for the 62 size-class configuration. At the scale of the individual size-classes, the output is characterised by orders of magnitude oscillations in the concentration. However, as will be seen later on, the bulk properties of the model such as total phytoplankton biomass are more constrained.

Total nitrogen (TN) in surface layer in the simulation is relatively constant (Fig. 5), despite a downward flux of phytoplankton and protozoa due to sinking. The slope of the biomass size spectra appears to vary between a value of −0.9 and −1.0.

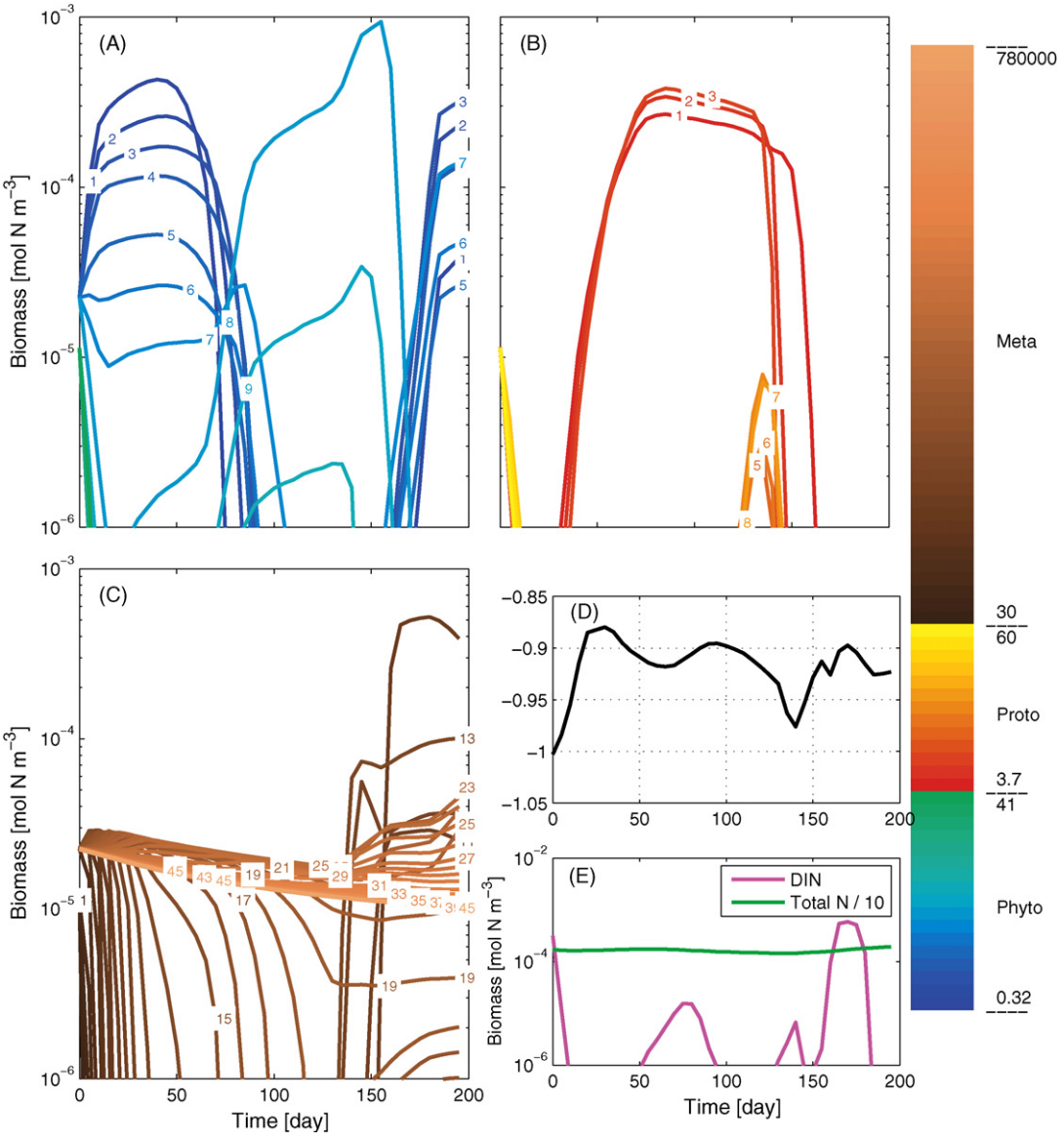

Fig. 5 – Concentration in the surface mixed layer of each size-class in the (A) phytoplankton, (B) protozoan and (C) metazoan groups for the 62 size-class configuration. Panel (D) shows the calculated slope of the biomass size-spectra determined as a Pareto distribution statistic. Panel (E) shows the dissolved inorganic nitrogen and total nitrogen. The size-class of each line can be determined using the colour bar on the right to identify functional group and relative size. The numbers on the colour bar refer to the radii of smallest and largest size-class in the spectra in μm. The line numbering on the graph refers to size-class within each functional group (i.e 1 is the smallest metazoan size-class and 45 is the largest).

4.1. *Sensitivity to initial conditions*

An ensemble of runs on the 62 size-class configuration have been undertaken with an initial slope of the biomass size spectrum of −1.0, but small perturbation in each individual size-class. The perturbations are based on a uniform distribution with a standard deviation of 0.064 of the original mass, and normalised such that the total mass of all size-classes is identical for all simulations. Fig. 6 shows the paths of phytoplankton, protozoan and metazoan biomass from the small initial perturbations for the first 250 days of the simulations. The simulations initially have very similar paths, but begin to diverge at about 120 days. The divergence in paths appears to be initiated by the blooming of phytoplankton with a radius greater than 2 μm, and quickly affects the protozoan and metazoan biomass.

Inspection of the trajectories of particular size-classes shows that the instability at Day 120 is caused by phytoplankton size-class 8 (P8) and its predators. Fig. 7 plots the phase space for state variables dissolved inorganic nitrogen, biomass of P8 ($r = 2.6\,\mu m$), and the sum of biomass of the grazers on P8. These grazers are protozoan size-classes 5 ($r = 9.4\,\mu m$) to 13 ($r = 60\,\mu m$) and metazoan size-classes 1 ($r = 30\,\mu m$) to 10 ($r = 242\,\mu m$). At Day 120 the trajectories are almost identical, and by Day 190 all have returned to a similar trajectory. In general the trajectories follow an initial path of increasing P8

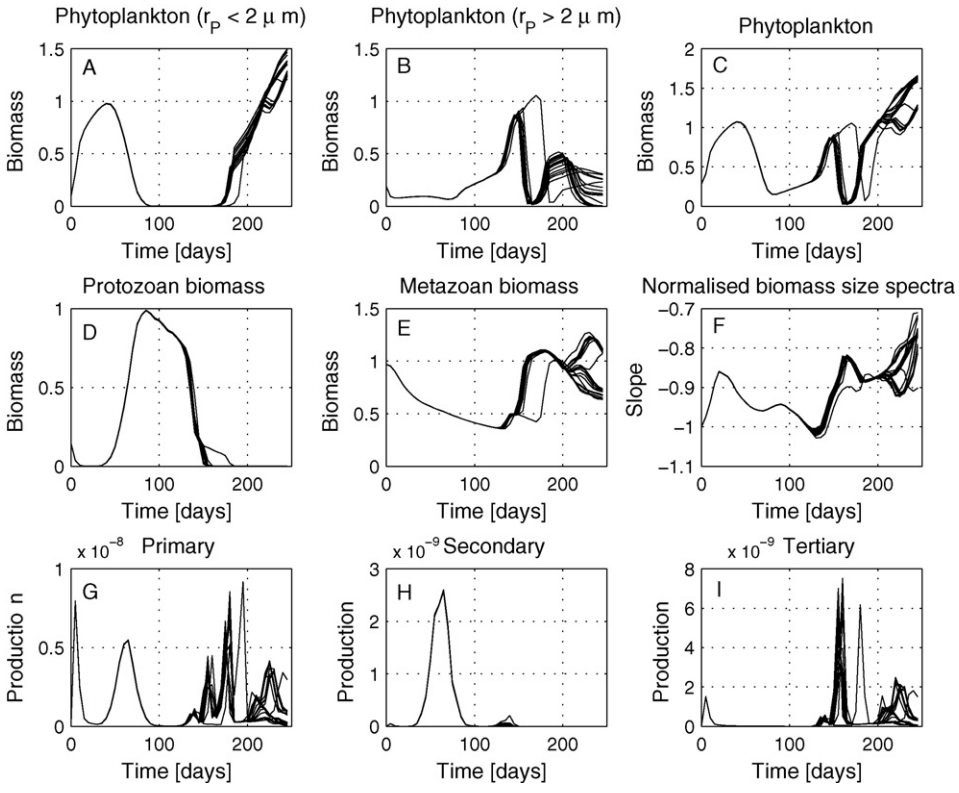

Fig. 6 – The first 250 days of an ensemble of 20 simulations for the 62 size-class configuration with small perturbations of initial conditions. Results shown are (A) biomass of phytoplankton with a radius less than 2 μm, (B) biomass of phytoplankton with a radius greater than 2 μm, (C) total phytoplankton biomass, (D) total protozoan biomass, (E) total metazoan biomass, (F) the slope of the normalised biomass size spectra, (G) the growth of phytoplankton, (H) the growth of protozoa, and (I) the consumption (for growth) of metazoa. Biomass is in mmol N m^{-3} and production is in mol N m^{-3} s^{-1}.

biomass until approximately Day 150, followed by an increase in grazer biomass and decreased P8 biomass, which is accompanied by an increase in DIN. The grazer biomass saturates at approximately 5×10^{-4} mol N m^{-3}, followed by a decrease in DIN, due to uptake by other phytoplankton size-classes, and finally the grazer biomass begins to crash.

The trajectories of the 20 ensemble runs begin to diverge around Day 120. The divergence occurs both in phase space and in time (Fig. 7). In particular, two trajectories (black in Fig. 7) have a larger increase in grazers of P8 than the remaining 18 (colour in Fig. 7) trajectories between Days 120 and 150. This delays the increase in P8 biomass, as shown by the Day 150 marker occurring at a lower biomass than for the other trajectories, and allows a greater P8 biomass to eventually be reached. The grazer maximum that follows is much later in the two black trajectories compared to the 18 coloured trajectories, and is slightly higher.

Fig. 8 demonstrates that after a few 100 days, the simulations can take drastically different paths (despite only tiny changes in initial conditions). The initial change in trajectories in this case precipitated by the predator–prey interactions of phytoplankton size-class 8 quickly propagate to larger size-classes, resulting in divergent paths of bulk properties such as total phytoplankton biomass later on in the simulations. It will be left to future work to investigate the behaviour at timescales greater than 100 days. At the present it sufficient to note that (1) while some of the paths may appear very different, the slope of the normalised biomass size spectra remains in a realistic range and (2) it is reasonable to expect a sensitivity to initial conditions in pelagic ecosystems. The remaining investigations in this paper will be restricted to the first 100 days of the simulations to minimise interacting effects of sensitivity to initial conditions, model resolution, biological boundary conditions, and allometric relationships.

4.2. *Sensitivity to size-resolution*

Further analysis of the size-resolved approach involves investigating the effect of changing the resolution of the biological configuration. The model equations, and the allometric relationships from which physiological rates are determined, are unchanged by model resolution. At high enough resolution, the output of the model averaged over a sufficiently large size range should be insensitive to further increases in resolution.

The sensitivity of the biological model to the resolution of size-classes was assessed by undertaking simulations with one quarter, one half, twice and four times the resolution of the 62 size-class configuration detailed in Section 3.7. The phytoplankton, protozoan and metazoan grids retain their original smallest and largest size-classes in all simulations, but the interval between size-classes is altered, resulting in 17, 32, 62, 123 and 245 size-class configurations, respectively

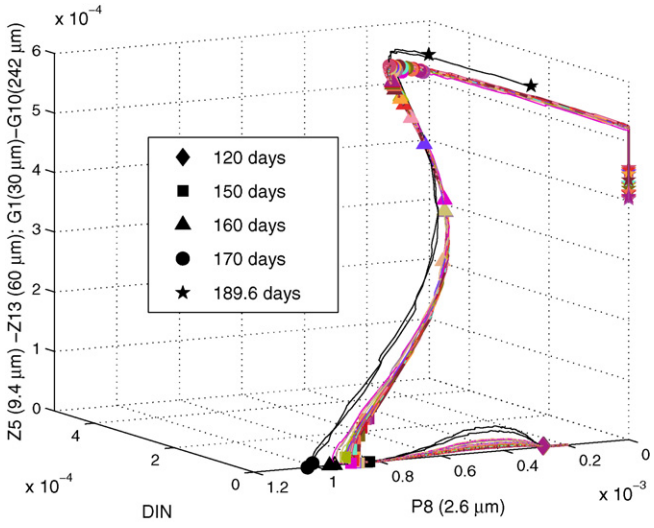

Fig. 7 – Phase space for state variables phytoplankton size-class 8 ($r = 2.6$ μm), dissolved inorganic nitrogen (DIN), and the sum of the grazers on phytoplankton size-class 8—protozoa 5 ($r = 9.4$ μm) to 13 ($r = 60$ μm) and metazoa 1 ($r = 30$ μm) to 10 ($r = 242$ μm). Each line is one of a 20 ensemble run of the 62 size-class configuration with slightly varying initial conditions, with the output given every 0.2 days from Day 100 to 190. The coloured diamond, square, triangle, circle and star symbols mark time points along each trajectory.

(Fig. 9). Note that when halving and halving again the 62 size-class configuration, the metazoan grid is out of alignment with the protozoan and phytoplankton grids. In this sense the 17 and 32 class configurations are only nominally 17 and 32 configurations, as they actually contain organisms at 18 and 34 size-classes, respectively. When increasing the resolution, this misalignment artifact does not occur.

Fig. 10 graphs a time series of the DIN, total phytoplankton biomass, total protozoan biomass and total metazoan biomass for the five biological configurations over the first 100 days of a simulation. The behaviour of the 17 and 32 size-class configurations are quite different to the higher resolution configurations. The 62, 123 and 245 size-class configurations follow similar tracks, demonstrating a convergence of results with increasing resolution. Achieving a tight convergence at high resolution is somewhat hampered by the different initial biomass held in each functional group—a result of the way the resolution is doubled. Nonetheless, after 300 days (not shown), the 123 size-class simulation behaves much more like the 245 size-class configuration than the 62 size-class configuration.

The major source of error in the discretisation of size-classes is the ability of the model to resolve the appropriate range of prey for a particular predator species. For the 17 size-class configuration, the predator of radius 7.7 cm has two prey species with radii that are 40.2 and 16.0 times smaller. For the 32 size-class configuration, the same size predator has four prey species, with a range between 64 and 16 times smaller. For the 62, 123 and 245 size-class configurations, the same predator has 9 (range 80.6–12.7 smaller), 19 (range 90.5–11.3 smaller) and 38 (90.5–10.7 smaller) prey species, respectively.

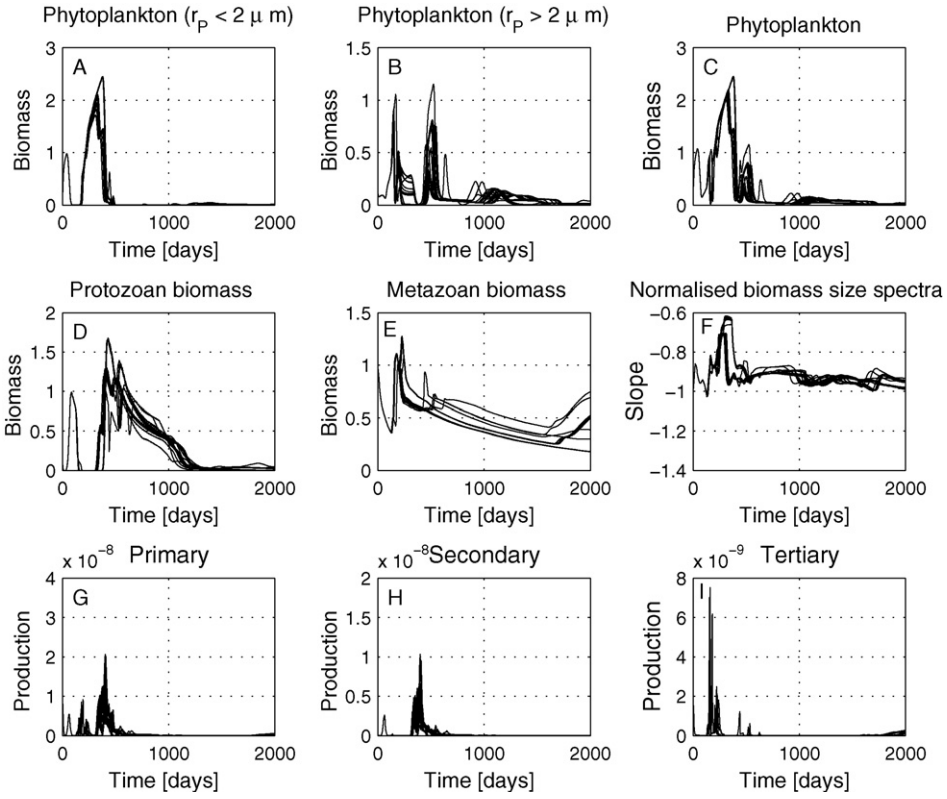

Fig. 8 – The first 2000 days of an ensemble of 20 simulations for the 62 size-class configuration with small perturbations of initial conditions. For further details see Fig. 6.

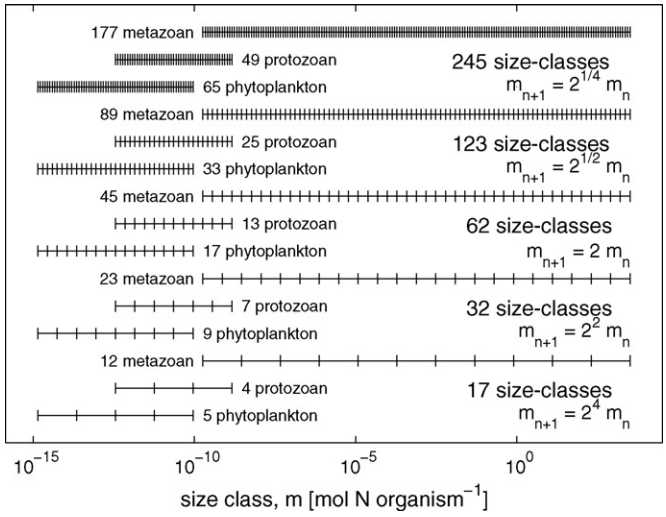

Fig. 9 – The biological size-classes for five different resolution configurations. The boundaries of the phytoplankton, protozoan and metazoan grids are identical for all configurations, while the gap between classes is halved with each increase in grid resolution. The 17 and 32 size-classes grids are nominally 17 and 32 size-classes, as the mismatch between size-classes on the metazoan and protozoan grids (a result of requiring that the grids in the different resolutions all have the same boundaries) produces organisms at 18 and 33 size-classes, respectively.

As the resolution of model increases, the percentage of all metazoans that the 7.7 cm radii predator has in its diet is: 16.67, 17.39, 20.00, 21.35 and 21.47. It can be shown that for an infinitely-resolved configuration increasing by a factor of 2^x, where $x \to 0$, between size-classes, with prey ranges of 90.73–10.26 and the same smallest and largest metazoan classes, a predator will have a diet consisting of 21.43% of the metazoan classes. Furthermore, as the resolution increases, the diet range approaches the full range of 90.73 to 10.26 given in the allometric relationships (Table 3). The convergence of the simulations of the 123 and 245 size-class configurations occurs because the prey ranges, and fraction of the total metazoan biomass they represent, are almost identical.

From both numerical experiments and theoretical considerations, it appears that the minimum resolution at which the size-resolved approach can confidently be used is the 62 size-class configuration. With each doubling of the number of size-classes, the number of interactions between classes (and therefore computational time) increases by approximately a factor of four—two for the increasing number of classes, and a further two for the increasing number of prey in each predator's diet. Due to computational constraints, results presented in this paper will be restricted to the 62 size-class configuration with a 1D spatial resolution of 31 vertical layers. At this resolution, it is presently feasible to run the model for a number of years and to undertake a sensitivity analysis of all 21 allometric relationships (42 simulations ran simultaneously on a condor cluster of 2.8 GHz Intel chips at a speed of ~37 model days per cpu hour).

4.3. *Sensitivity to metazoan upper boundary condition*

A further test of the robustness of the size-resolved model approach is to consider the effect of altering the boundary conditions of the biological grid. The lower and upper boundaries of the phytoplankton and protozoans, and the lower boundary of the metazoan size-classes are zero flux, and have been specified based on identified size-ranges in the literature. As a result, altering these boundaries is probably not a very insightful exercise.

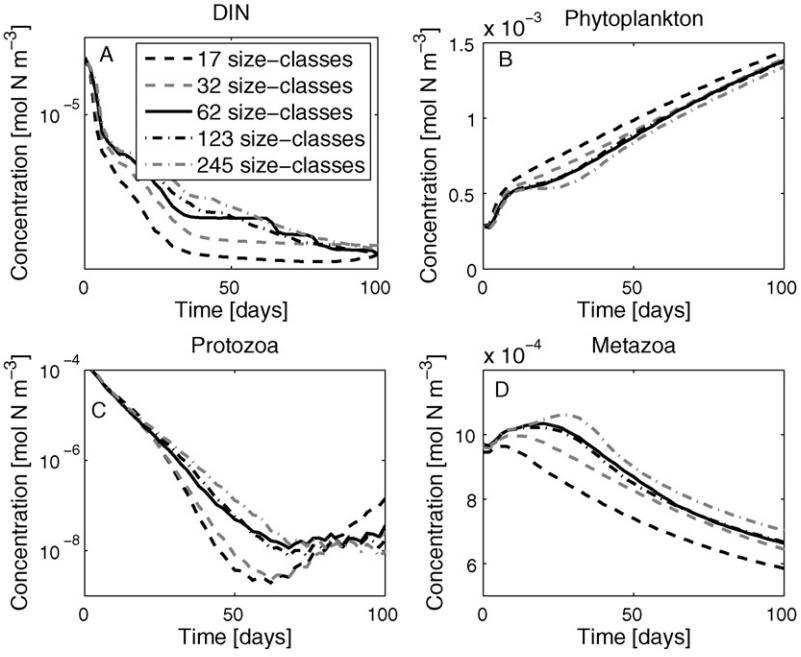

Fig. 10 – Concentration at the surface of (A) dissolved inorganic nitrogen, (B) total phytoplankton biomass, (C) total protozoan biomass and (D) total metazoan biomass for the 17, 32, 62, 123 and 245 size-class configurations.

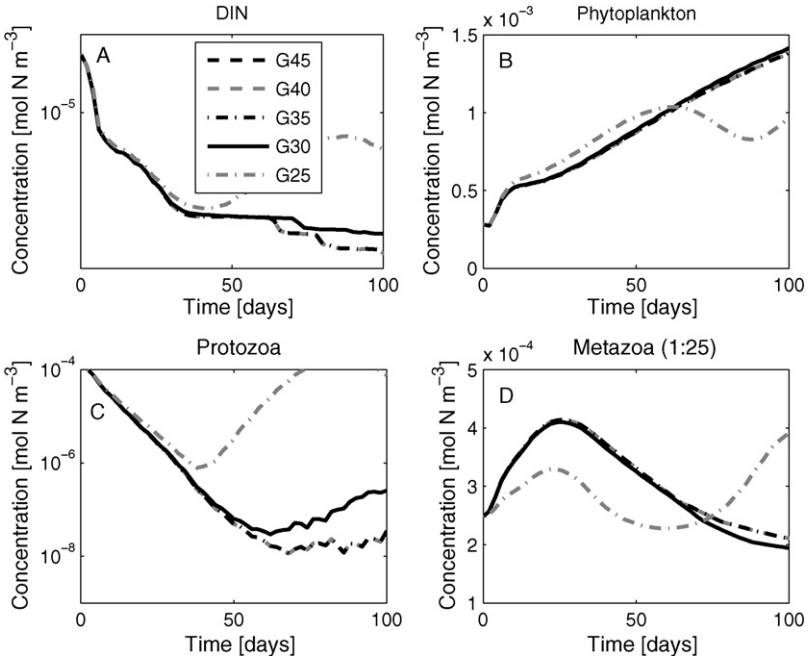

Fig. 11 – Concentration at the surface of (A) dissolved inorganic nitrogen, (B) total phytoplankton biomass, (C) total protozoan biomass and (D) total metazoan biomass in the first 25 size-classes when the upper metazoan boundary is unmoved (class 45 in the 62 size-class configuration) and moved to size-classes 40, 35, 30 and 25.

The upper boundary condition of the metazoa is important. Firstly it is the most poorly resolved biological boundary, being approximately 100 times smaller (by mass) than the largest marine animal, the blue whale *Balaenoptera musculus*. Secondly, it is an open boundary, with a quadratic mortality term relaxing the solution to a set slope of the NBSS. It is important to investigate how these shortcoming affect the solution of the model.

The upper metazoan boundary condition was moved progressively into the model interior (i.e. to smaller size-classes), and an assessment made of changes in bulk properties of the model. The boundary of the 62 size-class configuration is moved 5, 10, 15 and 20 size-classes lower, resulting in the metazoan boundary being at an ESR of 25, 7.8, 2.5 and 0.77 cm, respectively. In the 62 size-class configuration, with the boundary at an ESR of 0.77 cm, all of the predators of phytoplankton and protozoans are resolved. All size-classes are given the same initial conditions, but those beyond the boundary do not vary with time.

When the boundary is moved to the 25th or 30th metazoan size-class, the DIN, total phytoplankton, total protozoan and sum of the metazoan in the first 25 metazoan size-classes is different to that obtained with the boundary at the 45th metazoan size-class (Fig. 11c). For a boundary set at the 35th or 40th metazoan size-class, the solution is almost identical to that obtained with the boundary at the 45th metazoan size-class. For the prediction of total phytoplankton and protozoan biomass, and metazoan biomass smaller than the 25th metazoa size-class (ESR of 0.77 cm), a boundary at the 35th metazoan size-class has only a small influence in a 100-day simulation.

4.4. *Sensitivity analysis of allometric relationships*

A sensitivity analysis has been undertaken on the 62 size-class configuration by co-varying the coefficients of the allometric relationships plus and minus the standard error of the coefficients. This provides a measure of parameter sensitivity relative to the ability of the allometric relationships to capture the true size-dependence over the whole population of a particular functional group. As such it indicates the allometric relationships whose uncertainty is most limiting to the size-resolved approach.

The sensitivity of DIN, total phytoplankton biomass, total protozoan biomass and total metazoan biomass (Table 4) and a number of key biological processes (Table 5) in the surface layer, averaged over the period of 40–50 days, are reported. The sensitivity, in this case for total phytoplankton biomass, is given by:

$$\mathcal{S} = \frac{\left(\sum_1^{\mathcal{P}} \mathrm{P}\right)_{\text{allometric relationship} \pm \text{S.E.}}}{\left(\sum_1^{\mathcal{P}} \mathrm{P}\right)} \tag{23}$$

and similarly for other state variables and terms. The subscript allometric relationship ± SE refers to the co-varying of intercept and slope coefficients of each allometric relationship as described in Section 3.6.

DIN is most sensitive to the parameter describing the smallest size-class of prey available to a metazoan predator, $\Re_{\mathrm{G,max}}$, and the nitrogen content of a phytoplankton cell, $m_{\mathrm{P,N}}$ (Table 4). Other parameters which change the DIN concentration by more than 15% are the swimming velocity of phytoplankton, U_{P}, the maximum growth rate of phytoplank-

Table 4 – Sensitivity of functional groups to coefficients in allometric relationships

Parameter	DIN	Phytoplankton	Protozoa	Metazoa	NBSS slope
$m_{P,N}$	0.47 (1.84)	1.03 (0.96)	0.47 (1.67)	1.02 (0.99)	1 (1)
U_P	0.77 (1.73)	1.02 (0.95)	0.81 (1.53)	1 (1)	1 (1)
C	0.9 (0.94)	1.01 (1.01)	0.9 (0.94)	1 (1)	1 (1)
μ_P^{max}	1.07 (0.81)	1 (1.01)	1.08 (0.81)	1 (1)	1 (1)
w_P	0.99 (1)	1.01 (0.99)	0.99 (1)	1 (1)	1 (1)
$m_{Z,N}$	1.07 (0.93)	0.99 (1.01)	1.04 (0.91)	1 (1)	1.01 (0.99)
U_Z	0.91 (1.12)	1.01 (0.99)	0.93 (1.1)	1 (1)	1 (1)
μ_Z^{max}	1 (1)	1 (1)	1 (1)	1 (1)	1 (1)
w_z	1.03 (0.98)	1 (1)	1.03 (0.98)	1 (1)	1 (1)
γ_Z	1.36 (0.72)	0.97 (1.03)	1.39 (0.7)	1 (1)	1 (1)
$\Re_{Z,min}$	0.95 (1.03)	1 (1)	0.96 (1.03)	1 (1)	1 (1)
$\Re_{Z,max}$	0.98 (0.61)	1 (1.03)	0.91 (0.71)	1 (0.99)	1.02 (0.98)
$m_{G,N}$	1.11 (0.9)	0.99 (1.01)	1.1 (0.91)	1 (1)	1 (1)
U_G	1.06 (0.93)	0.99 (1.01)	1.05 (0.93)	1 (1)	1 (1)
μ_G^{max}	1.12 (0.85)	1 (1)	1.09 (0.87)	0.98 (1.02)	1 (1)
γ_G	0.81 (1.14)	1.01 (1)	0.82 (1.13)	1.02 (0.99)	1 (1)
$m_{C,\bigcirc}$	1 (1.01)	1 (1)	1 (1.01)	1 (1)	1 (1)
Λ	1 (1.01)	1 (1)	1 (1.01)	1 (1)	1 (1)
$\Re_{G,min}$	1.01 (1.51)	1 (0.97)	1.01 (1.46)	1 (0.98)	1 (1)
$\Re_{G,max}$	0.24 (2.63)	1.07 (0.87)	0.24 (2.42)	1 (1)	0.97 (1.02)

Sensitivity of dissolved inorganic nitrogen (DIN), total phytoplankton biomass, total protozoan biomass, total metazoan biomass and slope of the normalised biomass size spectra (NBSS) at the surface averaged over Days 40–50 to varying the allometric relationships by + and (–) the standard error in the 62 size-class configuration.

ton, μ_P^{max}, the yield of protozoa, γ_Z, the yield of metazoa, γ_G, the smallest size-class of prey available to a protozoan predator, $\Re_{Z,max}$, and the largest size-class of prey available to a metazoan predator, $\Re_{G,min}$.

The protozoan biomass has a similar sensitivity as DIN. In contrast, both phytoplankton and metazoan biomass are less sensitive to the allometric relationships. In part this can be explained by the larger range of size classes. For example, a shift to larger size classes of phytoplankton will not drastically change the biomass of phytoplankton. However, such a shift may limit the food source of protozoa, and change the concentration of DIN, as larger cells with smaller surface area to volume ratios are not able to draw nutrient concentrations as low as smaller phytoplankton. Phytoplankton biomass is most sensitive to the smallest size-class of prey available to a metazoan predator, $\Re_{G,max}$, while metazoan biomass is most sensitive to the maximum growth rate of metazoa, μ_G^{max}. The slope of the biomass size spectra is not very sensitive

Table 5 – Sensitivity of biological terms to coefficients in allometric relationships

Parameter	Phytoplankton growth	Protozoan growth	Metazoan consumption	Metazoan birth
$m_{P,N}$	0.57 (1.45)	0.55 (1.43)	1.23 (0.89)	1.33 (0.93)
U_P	0.8 (1.54)	0.79 (1.56)	0.98 (1.04)	0.98 (1.04)
C	0.91 (0.95)	0.91 (0.95)	1 (1)	1 (1)
μ_P^{max}	1.1 (0.8)	1.09 (0.81)	1.01 (0.99)	1.01 (1)
w_P	1 (0.99)	1 (0.99)	1 (1)	1 (1)
$m_{Z,N}$	1.06 (0.94)	1.05 (0.94)	1.23 (0.99)	1.36 (0.99)
U_Z	0.93 (1.1)	0.92 (1.1)	0.99 (1.01)	0.99 (1.01)
μ_Z^{max}	1 (1)	1 (1)	1 (1)	1 (1)
w_z	1.02 (0.98)	1.02 (0.98)	1 (1)	1 (1)
γ_Z	1.26 (0.77)	1.44 (0.67)	1.03 (0.97)	1.02 (0.98)
$\Re_{Z,min}$	0.96 (1.03)	0.96 (1.03)	0.99 (1)	1 (1)
$\Re_{Z,max}$	0.98 (0.67)	0.97 (0.64)	1.35 (0.94)	1.57 (0.96)
$m_{G,N}$	1.09 (0.91)	1.09 (0.91)	1 (0.99)	1.01 (0.99)
U_G	1.04 (0.94)	1.04 (0.94)	1.01 (0.99)	1.01 (0.99)
μ_G^{max}	1.11 (0.86)	1.11 (0.86)	1.09 (0.9)	1.18 (0.91)
γ_G	0.83 (1.12)	0.83 (1.12)	1.05 (0.94)	1.05 (0.96)
$m_{C,\bigcirc}$	1 (1.01)	1 (1.01)	1 (1)	1.06 (0.89)
Λ	1 (1)	1 (1)	1 (1)	1 (0.85)
$\Re_{G,min}$	1.01 (1.39)	1.01 (1.4)	1 (1.03)	1 (1.04)
$\Re_{G,max}$	0.3 (1.96)	0.26 (1.94)	0.94 (1.08)	0.97 (1.09)

Sensitivity of phytoplankton growth, protozoan growth, metazoan consumption and metazoan birth at the surface averaged over Days 40–50 to varying the allometric relationships by + and (–) the standard error in the 62 size-class configuration.

to any parameters, with the most sensitive parameter being $\Re_{G,max}$.

The sensitivity of phytoplankton growth, protozoan growth, metazoan consumption and metazoan birth are given in Table 5. It is interesting to note that metazoan consumption and metazoan birth are far more sensitive to the allometric relationships than the metazoan biomass. In part this is a consequence of metazoan biomass changing over long time scales. Metazoan consumption and birth is most sensitive to the smallest size-class of prey available to a protozoan predator, $\Re_{Z,max}$, and the nitrogen content of phytoplankton, $m_{P,N}$, and protozoa, $m_{Z,N}$.

5. Discussion

The size-resolved model developed in this paper has similarities with a variety of existing pelagic ecosystem models. It contains a small number of functional groups like trophically based NPZ models (Edwards and Brindley, 1996), a range of sizes of phytoplankton and zooplankton in common with size-structured models (Gin et al., 1998), the use of physical descriptions of limits to biological processes such as used in Baird and Emsley (1999) or Lewis (2003), and, the consideration of life-cycles such as found in age-structured models (James et al., 2003). In developing the size-resolved model, these approaches have been combined and, in many cases abridged, in order to create a model which concentrates on capturing the size-distribution of biomass.

The model contains just light and one nutrient limitation of photosynthesis, three functional groups, and a small set of equations describing the growth, mortality, and reproduction of plankton. In particular, the model equations and parameters are formulated independently of the number of size-classes resolved. This greatly reduces the complexity of the formulation when compared to size-structured models that specify each interaction separately. The application, however, is highly resolved. For example, in the 62 size-class configuration, the 5th smallest metazoan engages in 28 biological interactions alone (Fig. 1.), with the total number of planktonic interactions exceeding 1000. The 245 size-class configuration has well over 4000 interactions. As such, this approach can far exceed the complexity of even elaborate diagrammatic representation of pelagic food webs (Nybakken, 2001), and associated size-structured models.

The size-based approach. In Baird et al. (2004) a pelagic ecosystem model with bio-mechanical or physical descriptions of key biological processes is presented for one phytoplankton and one zooplankton size-class. An advantage of this approach was the reduction in the number of parameters typical of most pelagic ecosystem models, leaving the radii of a phytoplankton and zooplankton as the main parameters. From these radii, most other biological parameters could be derived. Nonetheless, the model remained sensitive to the choice of the plankton radii—a considerable problem since the radii most representative of a particular process in a pelagic ecosystem is likely to change temporally and spatially.

The model presented here removes the need to specify plankton radii. Plankton size becomes part of the biological grid, and no longer a model parameter. The number of size-classes represents the resolution of the model, in the same way as the number of spatial grid cells specifies the spatial resolution of a hydrodynamic model. With such a perspective, the parameters of the model becomes the coefficients of the allometric relationships, and the major problem of the trophically based biomechanical model of Baird et al. (2004) is overcome.

Assessment of model robustness. The size-resolved model allowed two tests of its approach that are difficult to undertake in size- or trophically structured models. Numerical experiments have shown that within the assumptions of the size-resolved model, the predictions of the 62 size-class configuration in size-classes smaller than 0.77 cm ESR are relatively insensitive to the coarseness of the grid, or the presence of a boundary at an ESR of 78 cm. Trophic and size-structured models are always open to general criticisms that the equations do not include sufficient state variables to represent the ecosystem, or that the coefficients and/or form of the higher-order closure term can potentially affect the model solution. In contrast, the effects of lack of resolution or higher order-closure terms in the size-resolved model have been carefully assessed, and shown to be small. This is not to say that the size-resolved model captures more aspects of a pelagic ecosystem than a size or trophically structured models. Rather, it simply demonstrates that for capturing the size-distribution of biomass for which it was formulated, it has sufficient resolution.

Sensitivity to allometric relationships. One of the most important results from this study of the size-resolved model is to determine which allometric relationships are most limiting to this approach. The sensitivity analysis shows that the most sensitive parameters relative to our knowledge of their values are the smallest size-class of prey available to a metazoan predator, $\Re_{G,max}$, and the nitrogen content of a phytoplankton cell. It is worth noting that these parameters come from small samples sizes relative to other parameters (Tables 2 and 3). To improve the performance of the size-resolved model, and our general understanding of size distribution of biomass in pelagic ecosystems, the most critical investigations to undertake would be on diet ranges of metazoan predators, such as those undertaken by Hansen et al. (1994).

Another feature that arises from the sensitivity analysis is the interdependence of all trophic levels. As noted above, the most sensitive parameter is the smallest size-class of prey available to a metazoan predator, $\Re_{G,max}$. Perhaps surprisingly, $\Re_{G,max}$ affects phytoplankton growth and protozoan growth more than metazoan consumption and birth. This occurs because $\Re_{G,max}$ changes the size-distribution of biomass, as shown by the NBSS (Table 5), affecting all components of the ecosystem.

Sensitivity to initial conditions The model output is sensitive to initial conditions, a necessary, although not sufficient, condition for chaotic behaviour. Sensitivity to initial conditions has been long been known in deterministic non-linear models of physical (Lorenz, 1963) and biological (May, 1976) systems, and there is every reason to expect that it might be a property of pelagic ecosystems. That the deterministic model behaves in such a manner places limitations on its use for prognostic modelling. The uncertainty given to the initial conditions of the state variables in the 20 ensemble runs is much less than the uncertainty with which the size-distribution of biomass

is likely to be known for any particular application. As such, the model cannot be used to predict the time-evolution of any particular size-class, and limitations exist for the prediction of even the total biomass of phytoplankton, protozoa or metazoa at time-scales greater than 100 days. Nonetheless, the general size-distribution of biomass, as defined by the normalised biomass size spectra, may be predictable on longer time-scales (much like the ability to predict weather for only for a few days, but climate over geological timescales). Even if the obstacles of a highly non-linear system prove too great for prognostic modelling at all, the size-resolved model may prove a useful diagnostic modelling tool.

Inherent limitations. The size-resolved approach has significant limitations, of which two seem the most important. Firstly, there is an inability to distinguish between organisms of the same size, but with different properties, such as that between a diatom and a coccolithophore, a dinoflagellate and a ciliate, or a copepod and a krill larva. Or even between an adult copepod and a larval fish. For example, the simple parameterisation used for predator searching behaviour in larger metazoans (Eq. (11)) does not consider the range of abilities to sense chemical and hydromechanical signals, or the various behavioural responses to these cues, that have evolved in the pelagic environment (Kiørboe and Bagøien, 2005). Another example can be seen in the allometric relationship for metazoan swimming (Fig. 3). The swimming speeds of the grouping rotifers, larvae and copepods have a different size-dependency (apparently little size-dependency) to that of the metazoans as a whole. Without resolving this group as a distinct functional group, it is not possible to include the differing size-dependency.

Secondly, the sensitivity analysis demonstrated the importance of the size-range of prey of protozoa and metazoa in the model formulation. In many circumstances, feeding preference on the basis of non-size based characteristics is also important. These additional complexities could be included in the size-resolved approach, although it may turn out that a trophic-based approach would be better suited to this task.

Further improvements to the size-resolved model. It is worth noting that this paper includes only a subset of the size-based relationships that are recorded in the literature. Other processes which have known size dependencies include swimming efficiency, schooling behaviour and turbulence production by animals (Huntley and Zhou, 2004), as well as more complex size-based considerations of grazing and reproductive strategies.

Given that predator–prey ratios are critical for the model, and that allometric relationships do not explain the variations of these properties within metazoan and protozoan groups, it may be helpful to further increase the number of functional groups. For example, salps could be considered a separate group of metazoans, due to their importance in biogeochemical cycles, and their extremely large predator–prey ratios (Andersen, 1998).

Conclusion and future work. A pelagic ecosystem model has been developed that resolves the size-distribution of biomass. Properties of the size-resolved approached are used to show that it is robust to changes in both resolution and biological boundary conditions. A sensitivity analysis illustrates where a lack of knowledge from laboratory parameterisations is most likely to cause problems in applying the model to oceanographic problems. The approach appears to avoid two of the most significant problems with classical models—namely a proliferation of model parameters with increasing complexity, and a need to change the model formulation for every change in model complexity.

Future work on this approach will involve coupling the size-resolved model to 2D and 3D physical models, in order to assess model size-distributions against observations. Furthermore, while the numerical experiments undertaken here provide coarse insights into the behaviour of the model, much will be learnt by a more complete dynamical analysis.

Acknowledgements

This research was funded by ARC Discovery Projects DP0557618 held by M.E. Baird and DP0209193 held by I.M. Suthers and M.E. Baird. We thank John Murray for organising the Mathematical Biology workshop at the School of Mathematics and Statistics (UNSW) that contributed to the development of this work, and Peter Blennerhassett, Bruce Henry and David Warton for helpful insigths. The use of the Australian Partnership for Advanced Computing (APAC) supercomputer, and the scientific programming support of Clinton Chee (High Performance Computing Unit, UNSW), Martin Thompson (School of Mathematics) and Patrick Timko are gratefully acknowledged. The physical configuration is based on earlier work with Peter Oke and Jason Middleton. We thank Alan Blumberg and George Mellor for the free availability of the Princeton Ocean Model.

Appendix A. Computational methodologies in the biological submodule

A.1. Integration schemes

Most of the biological equations are formulated as a set of ordinary differential equations (ODEs), while the advection and diffusion of biological tracers is formulated as a set of partial differential equations (PDEs). This type of advection–diffusion-reaction equation is typically solved by splitting the integration solution, and integrating the advection, diffusion and reaction equations sequentially (Baird et al., 2004).

The growth of individuals between size-classes is formulated as a PDE. This creates an awkward set of equations to solve as the biological equations become a coupled set of ODEs and PDEs. To incorporate the discretisation of the PDE within the ODE solver, a simple first-order upwind finite difference scheme is employed, with biomass moving only from smaller to larger size-classes, such that:

$$\frac{G_g^{n+1} - G_g^n}{\Delta t} = \frac{m_{g-1} g_{g-1} G_{g-1}}{(1/2)(\Delta m_{g-1} + \Delta m_g)} - \frac{m_g g_g G_g}{(1/2)(\Delta m_g + \Delta m_{g+1})} \quad \text{(A.1)}$$

with boundary conditions of zero flux at the smallest and largest size-class. Given that the quantity of biomass moved between size-classes over a timestep (60 s) is small relative

to the amount of biomass within the size-class, this simple approximation is sufficient.

The partial differential equations (PDEs) describing advection of biological tracers are integrated using two iterations of a positive definite advection scheme (Smolarkiewicz, 1984). The ordinary differential equations (ODEs) describing biological transformations are integrated using an adaptive 5th order Cash–Karp Runge–Kutta method (Press et al., 1992) with an absolute tolerance of 10^{-12} mol N m^{-3} for N, P and Z and 10^{-12} for R_N and R_I.

Appendix B. Supplementary data

Supplementary data associated with this article can be found, in the online version, at doi:10.1016/j.ecolmodel.2006.11.025.

REFERENCES

Andersen, V., 1998. Salps and pyrosomid blooms and their importance in biogeochemical cycles. In: Bone, Q. (Ed.), The Biology of Pelagic Tunicates. Oxford University Press, pp. 125–137.

Armstrong, R.A., 1999. An optimization-based model of iron-light-ammonium colimitation of nitrate uptake and phytoplankton growth. Limnol. Oceanogr. 44, 1436–1446.

Armstrong, R.A., 2003. A hybrid spectral representation of phytoplankton growth and zooplankton response: the control rod model of planktonic interaction. Deep-Sea Res. II 50, 2895–2916.

Baird, M.E., Emsley, S.M., 1999. Towards a mechanistic model of plankton population dynamics. J. Plankton Res. 21, 85–126.

Baird, M.E., Oke, P.R., Suthers, I.M., Middleton, J.H., 2004. A plankton population model with bio-mechanical descriptions of biological processes in an idealised 2-D ocean basin. J. Mar. Syst. 50, 199–222.

Banse, K., Mosher, S., 1980. Adult body mass and annual production/biomass relationships of field populations. Ecol. Monogr. 50, 355–379.

Batchelor, G.K., 1980. Mass transfer from small particles suspended in a turbulent fluid. J. Fluid Mech. 98, 609–623.

Blumberg, A.F., Mellor, G.L., 1987. A description of a three-dimensional coastal ocean circulation model. In: Heaps, N. (Ed.), Three-dimensional Coastal Ocean Models. American Geophysical Union, pp. 1–15.

Bonnet, D., Carlotti, F., 2001. Development and egg production in *Centropages typicus* (Copepoda: Calanoida) fed different food types: a laboratory study. Mar. Ecol. Prog. Ser. 224, 133–148.

Caparroy, P., Thygesen, U.H., Visser, A., 2000. Modelling the attack success of planktonic predators: patterns and mechanisms of prey size selectivity. J. Plankton Res. 22, 1871–1900.

Edwards, A.M., Brindley, J., 1996. Oscillatory behaviour in a three-component plankton population model. Dynam. Stabil. Syst. 11, 347–370.

Edwards, A.M., Yool, A., 2000. The role of higher predation in plankton population models. J. Plankton Res. 22, 1085–1112.

Edwards, C.A., Batchelder, H.P., Powell, T.M., 2000. Modeling microzooplankton and macrozooplankton dynamics within a coastal upwelling system. J. Plankton Res. 22, 1619–1648.

Fasham, M.J.R., 1993. Modelling the marine biota. In: Heimann, M. (Ed.), The Global Carbon Cycle. Springer-Verlag, New York, pp. 457–504.

Fenchel, T., 1974. Intrinsic rate of natural increase: the relationship with body size. Oecologia 14, 317–326.

Finkel, Z.V., 2001. Light absorption and size scaling of light-limited metabolism in marine diatoms. Limnol. Oceanogr. 46, 86–94.

Finkel, Z.V., Irwin, A.J., 2000. Modeling size-dependent photosynthesis: light absorption and the allometric rule. J. Theor. Biol. 204, 361–369.

Gentleman, W., 2002. A chronology of plankton dynamics in silico: how computer models have been used to study marine ecosystems. Hydrobiologica 480, 69–85.

Gillooly, J.F., 2000. Effect of body size and temperature on generation time in zooplankton. J. Plankton Res. 22, 241–251.

Gin, K.Y.H., Guo, J., Cheong, H.-F., 1998. A size-based ecosystem model for pelagic waters. Ecol. Model. 112, 53–72.

Graham, L.E., Wilcox, L.W., 2000. Algae. Prentice Hall.

Hansen, B., Bjornsen, P.K., Hansen, P.J., 1994. The size ratio between planktonic predators and prey. Limnol. Oceanogr. 39, 395–403.

Hansen, P.J., Bjornsen, P.K., Hansen, B.W., 1997. Zooplankton grazing and growth: scaling within the 2–2,000 μm body size range. Limnol. Oceanogr. 42, 687–704.

Heath, M.R., 1995. Size spectrum dynamics and the planktonic ecosystem of Loch Linnhe. ICES J. Mar. Sci. 52, 627–642.

Hein, M., Pedersen, M.F., Sand-Jensen, K., 1995. Size-dependent nitrogen uptake in micro- and macroalgae. Mar. Ecol. Prog. Ser. 118, 247–253.

Huntley, M.E., Zhou, M., 2004. Influence of animals on turbulence in the sea. Mar. Ecol. Prog. Ser. 273, 65–79.

Jackson, G.A., 1995. Coagulation of marine algae. In: Huang, C.P., O'Melia, C.R., Morgan, J.J. (Eds.), Aquatic Chemistry: Interfacial and Interspecies Processes. American Chemical Society, Washington, DC, pp. 203–217.

James, A., Pitchford, J.W., Brindley, J., 2003. The relationship between plankton blooms, the hatching of fish larvae, and recruitment. Ecol. Model. 160, 77–90.

Kerr, S.R., Dickie, L.M., 2001. The Biomass Spectrum. Columbia University Press, New York.

Kiørboe, T., 1993. Turbulence, phytoplankton cell size, and the structure of pelagic food webs. Adv. Mar. Biol. 29, 1–72.

Kiørboe, T., Bagøien, E., 2005. Motility patterns and mate encounter rates in planktonic copepods. Limnol. Oceanogr. 50, 1999–2007.

Kiørboe, T., Sabatini, M., 1995. Scaling of fecundity, growth and development in marine planktonic copepods. Mar. Ecol. Prog. Ser. 120, 285–298.

Kirk, J.T.O., 1994. Light and Photosynthesis in Aquatic Ecosystems, 2nd ed. Cambridge University Press, Cambridge.

Lewis, D.M., 2003. Planktonic encounter rates in homogeneous isotropic turbulence: the case of predators with limited fields of sensory preception. J. Theor. Biol. 222, 73–97.

Lorenz, E.N., 1963. Deterministic non-periodic flow. J. Atmos. Sci. 20, 130–141.

Marshall, A.J., Williams, W.D. (Eds.), 1972. Textbook of Zoology Invertebrates, 7th ed. Macmillan, London.

May, R.M., 1976. Simple mathematical models with very complicated dynamics. Nature 261, 459–467.

Moloney, C.L., Field, J.G., 1991. The size-based dynamics of plankton food webs. I. A simulation model of carbon and nitrogen flows. J. Plankton Res. 13, 1003–1038.

Morel, A., Ahn, Y., Partensky, F., Vaulot, D., Claustre, H., 1993. *Prochlorococcus* and *Synechococcus*: a comparative study of their optical properties in relation to their size and pigmentation. J. Mar. Res. 51, 617–649.

Mullin, M.M., Sloan, P.R., Eppley, R.W., 1966. Relationship between carbon content, cell volume and area in phytoplankton. Limnol. Oceanogr. 11, 307–311.

Nybakken, J.W., 2001. Marine Biology: An Ecological Approach, 5th ed. Benjamin Cummings, San Francisco.

Peters, R.H., 1983. The Ecological Implications of Body Size. Cambridge University Press.

Platt, T., Denman, K., 1977. Organisation in the pelagic ecosystem. Helgoländer wiss Meeresun. 30, 575–581.
Press, W.H., Flannery, B.P., Teukolsky, S.A., Vetterling, W.T., 1992. Numerical Recipes in Fortran 77: The Art of Scientific Programming, 2nd ed. Cambridge University Press.
Redfield, A.C., Ketchum, B.H., Richards, F.A., 1963. The influence of organisms on the composition of sea-water. In: Hill, N. (Ed.), The Sea, 2nd ed. Wiley, pp. 26–77.
Sheldon, R.W., Prakash, A., Sutcliffe, W.H., 1972. The size distribution of particles in the ocean. Limnol. Oceanogr. 17, 327–340.
Silvert, W., Platt, T., 1978. Energy flux in the pelagic ecosystem: a time-dependent equation. Limnol. Oceanogr. 23, 813–816.
Smayda, T.J., 1970. The suspension and sinking of phytoplankton in the sea. Oceanogr. Mar. Biol. Ann. Rev. 8, 353–414.
Smolarkiewicz, P.K., 1984. A fully multidimensional positive definite advection transport algorithm with small implicit diffusion. J. Comput. Phys. 54, 325–362.
Sommer, U., 1988. Some size relationships in phytoflagellate motility. Hydrobiologia 161, 125–131.
Steele, J.H., Henderson, E.W., 1981. A simple plankton model. The Am. Nat. 117, 676–691.
Tang, E.P.Y., 1995. The allometry of algal growth rates. J. Plankton Res. 17, 1325–1335.
Taylor, A.H., Stephens, J.A., 1993. Diurnal variations of convective mixing and the spring bloom of phytoplankton. Deep-Sea Res. II 40, 389–408.
Ware, D.M., 1978. Bioenergetics of pelagic fish: theoretical change in swimming speed and ration with body size. J. Fish. Res. Board Can. 35, 220–228.
Zhou, M., 2006. What determines the slope of a plankton biomass spectrum. J. Plankton Res. 28, 437–448.
Zhou, M., Huntley, M.E., 1997. Population dynamics theory of plankton based on biomass spectra. Mar. Ecol. Prog. Ser. 159, 61–73.